

Article

Thermal Analysis of Shell-and-Tube Thermoacoustic Heat Exchangers

Mohammad Gholamrezaei * and Kaveh Ghorbanian

Department of Aerospace Engineering, Sharif University of Technology, Tehran 11365-8639, Iran; ghorbanian@sharif.edu

* Correspondence: gholamrezaei@ae.sharif.edu; Tel.: +98-21-66-02-27-31

Academic Editor: Kevin H. Knuth

Received: 7 June 2016; Accepted: 8 August 2016; Published: 16 August 2016

Abstract: Heat exchangers are of key importance in overall performance and commercialization of thermoacoustic devices. The main goal in designing efficient thermoacoustic heat exchangers (TAHXs) is the achievement of the required heat transfer rate in conjunction with low acoustic energy dissipation. A numerical investigation is performed to examine the effects of geometry on both the viscous and thermal-relaxation losses of shell-and-tube TAHXs. Further, the impact of the drive ratio as well as the temperature difference between the oscillating gas and the TAHX tube wall on acoustic energy dissipation are explored. While viscous losses decrease with d_i/δ_κ , thermal-relaxation losses increase; however, thermal relaxation effects mainly determine the acoustic power dissipated in TAHXs. The results indicate the existence of an optimal configuration for which the acoustic energy dissipation minimizes depending on both the TAHX metal temperature and the drive ratio.

Keywords: heat exchangers; thermoacoustics; shell-and-tube; acoustic energy; dissipation

1. Introduction

Today, thermoacoustic engines, coolers, and heat pumps are receiving more industrial interest. While thermoacoustic engines utilize heat to generate acoustic power, the thermoacoustic refrigerators consume the acoustic power to transfer heat from the cold reservoir. In general, there are two basic types of thermoacoustic systems: standing-wave [1] and travelling-wave [2] systems. Thermoacoustic systems have three distinct advantages: first, they have no moving parts and are simple in structure, have low manufacturing costs, and are highly reliable. Further, they are environmentally friendly due to the usage of inert gases as the working fluid. Additionally, heat-driven thermoacoustic devices can be driven by low quality energy sources such as waste heat and solar energy.

The main components of a thermoacoustic device are the stack/regenerators and the two heat exchangers (HXs) that are placed at both ends of the stack/regenerators in an acoustic network. Although steady flow heat exchangers are a mature technology, their design is of key importance in commercialization of thermoacoustic devices where the flow is oscillatory.

All engines and refrigerators must reject waste heat to the ambient temperature where the ambient heat sink is often available as a flowing water stream. Similarly, engines must also accept heat from a heat source at a higher temperature (i.e., burner, waste heat, solar energy, etc.).

The efficiency of thermoacoustic engines is defined as the ratio of produced acoustic power to the heat received by the system [3]. However, irreversible dissipation of acoustic power in different components of thermoacoustic engines due to the viscous and thermal relaxation losses is the main source for performance degradation. Two highly dissipative components of thermoacoustic engines are the regenerators/stacks and the heat exchangers. These components have recently been the subject of many studies for system performance optimization. Wu et al. [4] presented a generalized heat transfer model using a complex heat transfer exponent to optimize the performance of a thermoacoustic engine.

Zhibin and Jaworski [5] studied the role of configuration and geometrical dimensions of a regenerator on the acoustic power dissipation. The irreversibility of the porous thermoacoustic stacks in terms of entropy generation is analyzed by Tasnim et al. [6] Chaitou and Nika [7] considered the dependence of acoustic energy on parameters such as stack's hydraulic radius and stack position.

As pointed out, an optimum design of TAHXs is a critical and challenging task for commercialization of thermoacoustic devices. The relationship between the acoustic energy dissipation, the heat exchanger geometry as well as the operating conditions is of significant importance. In general, while different parallel plate, finned-tube, and shell-and-tube HXs configurations are commonly used, the present knowledge of acoustic energy dissipation in TAHXs is relatively limited. It should be emphasized that designing efficient TAHXs in terms of the required heat transfer rate, in addition to low acoustic energy dissipation, remains a challenge.

Ishikawa and Hobson [8] derived an analytical expression of the time averaged entropy generation in parallel plate HXs. Piccolo [9,10] developed a computational model for studying the entropy generation characteristics of TAHXs with plane fins of a standing-wave thermoacoustic device. Previous studies focused mostly on parallel plate and finned-tube HXs.

It should be pointed out that, in case of high-capacity refrigerators and engines, the thermal conductivity of solids is insufficient to carry the required heats without significant temperature differences; hence, advanced and likely complex heat exchangers have to be used to interweave the process fluid and the working gas, bringing them into intimate thermal contact. A shell-and-tube heat exchanger system is the classical approach [11].

The present paper is focused on the shell-and-tube heat exchanger design of thermoacoustic systems and will investigate the relationship between the acoustic energy dissipation, viscous loss, thermal relaxation loss, and heat exchanger geometry. Much of the motivation behind the current work is driven by the interest as to whether there is a theoretical "optimum" of these parameters and/or the optimum of their combination for a specific operating point. Second, and more generally, the current research attempts to develop a simple but constructive methodology for comparison and evaluation of related heat exchangers at different operating conditions.

In this work, the heat exchangers are considered in the travelling-wave mode with ideal gases based on linear thermoacoustic theory. In this regard, heat exchangers with different geometries are investigated numerically and compared to each other. The dependence of the acoustic power dissipation on heat exchanger metal temperature and drive ratio for a fixed value of heat transfer rate is examined.

2. Theoretical Analysis

2.1. Thermal Modeling of Heat Exchangers

For heat transfer analysis, a local heat transfer coefficient is defined as the ratio of the heat transfer per unit area to the temperature difference between the surface and "bulk" fluid adjacent to the surface. However, in practice, a global heat transfer coefficient derived from a lumped analysis of the heat exchanger (UA-LMTD or effectiveness-NTU methods) is utilized [12].

The surface area, A_s , of the heat exchanger is expressed as

$$A_s = \frac{\dot{Q}}{T_{lm} U_i} \quad (1)$$

where \dot{Q} is the heat transfer rate, T_{lm} denotes the log-mean temperature and U_i is the overall heat transfer coefficient ($\text{W} \cdot \text{m}^{-2} \cdot \text{K}^{-1}$).

In the above equation, log-mean temperature difference model is used for thermal modeling of the shell-and-tube heat exchanger operating in the unsteady flow. The log-mean temperature difference for thermoacoustic shell-and-tube heat exchangers is formulated as follows:

$$T_{lm} = \frac{T_{w,o} - T_{w,i}}{\ln \left(\frac{T_m - T_{w,i}}{T_m - T_{w,o}} \right)} \quad (2)$$

where T_m is the gas mean temperature, $T_{w,i}$ and $T_{w,o}$ are the water inlet and outlet temperature, respectively.

In general, a shell-and-tube heat exchanger is considered with gas flowing through the tubes and water flowing over the tubes. The heat transfer in the heat exchanger involves the thermal resistance consisting of three parts: the resistance for heat transfer from the gas to the tube wall, the thermal resistance of the tube, and the resistance for heat transfer from the tube to the water. Therefore, the overall heat transfer coefficient is estimated based on the tube inner diameter according to

$$U_i = \left[\frac{1}{h_i} + N_t d_i (\ln(d_o/d_i) / 2\varepsilon) + \left(\frac{d_i}{d_o} \right) \frac{1}{h_o} \right]^{-1} \quad (3)$$

where d_o and d_i are the outside and inside tube diameters; h_i and h_o are the tube and shell-side heat transfer coefficient, respectively. Further, ε is the thermal conductivity of the tube. The shell-side heat transfer coefficient for water, h_o , may be recalled from classical heat exchanger textbooks, such as [12].

It should be pointed out that, for most thermoacoustic-related investigations, the heat transfer from the oscillatory gas to the heat exchanger inner surface area is mainly considered. In other words, the heat transfer across the tube wall and then further to the water is usually embedded. Thus, Equation (1) might be rewritten for heat transfer from the oscillatory gas to the tube wall as follows

$$A_s = \frac{\dot{Q}}{(T_m - T_s) h_i} \quad (4)$$

where T_s is the temperature of the tube wall at the gas side. This temperature is noted as the HX metal temperature in DeltaEC [13] and also as solid temperature in some TA studies [8,10]. Focusing on the heat transfer in oscillatory gas and employing T_s instead of T_w aids to eliminate the shell side parameters like the tube thickness, tube length and tube pitch which have a negligible influence on the acoustic energy dissipation.

The surface area, A_s , of a shell-and-tube heat exchanger is given as

$$A_s = N_t (\pi d_i L_t) \quad (5)$$

where N_t is the number of tubes and L_t is the length of the tubes. A_s is calculated according to heat transfer Equation (4).

Thermoacoustic Considerations

It is important to recognize that the problem of heat transfer from an acoustically oscillating gas medium to a solid surface is fundamentally different from that addressed in most discussions of compact heat exchangers that are based on steady unidirectional flow of fluid through the tubes of the heat exchanger. Indeed, TAHXs are distinguished by an oscillatory flow with zero mean velocity and this circumstance has two important implications [14].

The most significant difference between classical HXs and TAHXs is the acoustically oscillating gas parcels which only move a limited distance before reversing their direction of flow. The consequence of their periodic flow reversal is that one cannot arbitrarily increase the length of the heat exchange surfaces (tubes) in the direction of the flow to increase the effective surface area available for heat transfer. Thus, the optimum length, L_{TAHX} , of the heat exchanger should be of the order of the peak-to-peak displacement of the working gas acoustic displacement amplitude.

Another important aspect of TAHXs is that conventional steady flow heat transfer correlations cannot be directly applied for the estimation of the convective heat transfer coefficient, h_i , between the gas and the solid wall of TAHXs. Different approaches are currently proposed to overcome this limitation.

Swift [3,15] and Garrett [14] suggest an approximate estimation of heat transfer coefficient on the basis of a simple “boundary layer conduction heat transfer” model given as

$$h_i = \frac{k}{y_{eff}} \quad (6)$$

and

$$y_{eff} = \min[\delta_k, r_h] \quad (7)$$

$$r_h = d_i/4 \quad (8)$$

for shell-and-tube heat exchangers. The thermal conductivity of the gas is denoted by k and $\delta_k (= \sqrt{2k/\omega})$ is the thermal penetration depth—that is, the distance through which heat will diffuse in an acoustic cycle.

Mozurkewich [16], Peak et al. [17], Nsofar et al. [18] and Kamsanam et al. [19] also developed different numerical and experimental models of h_i for mostly parallel plate and finned-tube TAHXs. However, for shell-and-tube TAHXs, correlations of heat transfer coefficient are still limited. In this regard, Swift’s model [15] appears to be a sound approximation of h_i for oscillatory flow in shell-and-tube HXs especially when the flow in the tubes is laminar.

The tube side acoustic Reynolds number can be evaluated as follows

$$\text{Re}_d = \frac{\rho_m |u_1| d_h}{\mu} \quad (9)$$

where $d_h (= 4r_h)$ is the hydraulic diameter of the tube.

2.2. Acoustic Energy in TAHXs

According to the linear thermoacoustic theory [1,3], wave propagation in TAHXs is calculated using

$$\frac{dU_1}{dx} = -\frac{i\omega A_g}{\rho_m a^2} \left(1 + \frac{(\gamma - 1) f_\kappa}{1 + \epsilon_s} \right) p_1 \quad (10)$$

$$\frac{dp_1}{dx} = \frac{i\omega \rho_m}{(1 - f_v) A_g} U_1 \quad (11)$$

where U_1 and p_1 are oscillating volume velocity and pressure, respectively. A_g is the cross-sectional area of gas channels in the heat exchanger. f_v and f_κ are spatially averaged thermoviscous functions and are given in [1,3] in detail. It should be pointed out that, in this paper, thermoviscous functions for cylindrical geometry is considered for shell-and-tube TAHXs. γ , a , ϵ_s and ρ_m are the ratio of specific heat capacities, sound speed, correction factor for finite solid heat capacity, and mean density of the working gas, respectively.

Furthermore, A_g is expressed as

$$A_g = N_t \pi d_i^2 / 4 \quad (12)$$

The time averaged acoustic power $d\dot{E}_2$ produced in a length dx of the channel is given in complex notation in the general form as

$$\frac{d\dot{E}_2}{dx} = \frac{1}{2} \text{Re} \left[\tilde{U}_1 \frac{dp_1}{dx} + \tilde{p}_1 \frac{dU_1}{dx} \right] \quad (13)$$

Here, the tilde, “~”, indicates a complex conjugation. Subscript 2 indicates the second order quantity and Re denotes the real part of the complex number.

Substituting Equations (10) and (11) into Equation (13), one obtain as [3]:

$$\frac{d\dot{E}_2}{dx} = -\frac{r_v}{2} |U_1|^2 - \frac{1}{2r_\kappa} |p_1|^2 + \frac{1}{2} \text{Re} [g\tilde{p}_1 U_1] \quad (14)$$

In the above equation, the viscous resistance per unit length of the channel, r_v , the thermal relaxation conductance per unit length of the channel, $1/r_\kappa$, and the complex gain/attenuation constant for the volume flow rate, g , are defined as follows:

$$r_v = \frac{\omega \rho_m \operatorname{Im}[-f_v]}{A_g |1 - f_v|^2} \quad (15)$$

$$\frac{1}{r_\kappa} = -\frac{\gamma - 1}{\gamma(1 + \epsilon_s)} \frac{\omega A_g \operatorname{Im}[-f_\kappa]}{p_m} \quad (16)$$

and

$$g = \frac{(f_\kappa - f_v)}{(1 - f_\kappa)(1 - \sigma)(1 + \epsilon_s)} \frac{1}{T_m} \frac{dT_m}{dx} \quad (17)$$

Here, σ , p_m and T_m are the Prandtl number, mean pressure, and mean temperature of the working gas, respectively.

On the right hand side of Equation (14), regardless of the temperature gradient along the length of the channel, the first two terms represent viscous and thermal-relaxation dissipation, which always consume acoustic power. The third term denotes the acoustic power produced (or consumed) by the channel due to the axial temperature gradient depending on the magnitude and direction of the axial temperature gradient.

In TAHXs, it is mostly assumed that the length of the heat exchanger is short; therefore, T_m remains constant and there is no axial temperature gradient ($dT_m/dx = 0$), so the third term vanishes. Therefore, it will be more convenient to refer to $d\dot{E}_2/dx$ as a “net” time averaged acoustic power dissipated per unit length of the heat exchanger due to viscous and thermal relaxation loss (the first two terms of the RHS of Equation (14)).

To calculate the acoustic power dissipated in the heat exchanger, $d\dot{E}_2/dx$ is integrated over the length of the heat exchanger. Thus, \dot{E}_{diss} is written as

$$\dot{E}_{diss} = -\int_0^{L_{TAHX}} \frac{d\dot{E}_2}{dx} dx = \dot{E}_{diss,v} + \dot{E}_{diss,\kappa} \quad (18)$$

where $\dot{E}_{diss,v}$ and $\dot{E}_{diss,\kappa}$ represent viscous and thermal dissipation of acoustic power in the heat exchanger, respectively.

$$\dot{E}_{diss,v} = \int_0^{L_{TAHX}} \frac{\omega \rho_m \operatorname{Im}[-f_v]}{A_g |1 - f_v|^2} |U_1|^2 dx \quad (19)$$

$$\dot{E}_{diss,\kappa} = \int_0^{L_{TAHX}} -\frac{\gamma - 1}{2\gamma(1 + \epsilon_s)} \frac{\omega A_g \operatorname{Im}[-f_\kappa]}{p_m} |p_1|^2 dx \quad (20)$$

For shell-and-tube heat exchangers, replacing A_g with A_s in Equations (18) and (19), one may rewrite $\dot{E}_{diss,v}$ and $\dot{E}_{diss,\kappa}$ as follows

$$\dot{E}_{diss,v} = \int_0^{L_{TAHX}} \frac{4\omega \rho_m L_{hx} \operatorname{Im}[-f_v]}{d_i A_s |1 - f_v|^2} |U_1|^2 dx \quad (21)$$

$$\dot{E}_{diss,\kappa} = \int_0^{L_{TAHX}} -\frac{\gamma - 1}{2\gamma(1 + \epsilon_s)} \frac{\omega d_i A_s \operatorname{Im}[-f_\kappa]}{4p_m L_{hx}} |p_1|^2 dx \quad (22)$$

3. Results and Discussion

In this paper, \dot{E}_{diss} is used as an evaluation index for TAHXs. However, it is also important to understand both $\dot{E}_{diss,v}$ and $\dot{E}_{diss,\kappa}$ which provide an estimation of the total dissipation if integrated together. Therefore, for shell-and-tube heat exchangers, both $\dot{E}_{diss,v}$ and $\dot{E}_{diss,\kappa}$ are numerically

determined. The normalized tube diameter, d_i/δ_κ , is used for the analysis. All calculations are performed for helium as the working fluid ($\sigma = 2/3$, $\gamma = 5/3$).

According to Equations (1) and (21), the knowledge of heat transfer rate (\dot{Q}), gas mean temperature (T_m), TAHX metal temperature (T_s), and L_{TAHX} (which is equal to L_t in this paper) are required for numerical analysis. The gas mean temperature is determined in the design process of thermoacoustic systems. For example, in Backhaus and Swift's travelling-wave engine [2], the heat load of the ambient heat exchanger is 1614 W, the L_{TAHX} of the heat exchanger is 20 mm, and the gas mean temperature is 319 K at the middle of HX. The operating frequency is 84 Hz with helium at a mean pressure of 3.1 MPa as the working gas. In addition, the HX material is stainless steel. Parameters of the TAHX and the working conditions are presented in Table 1. In this paper, for the purpose of comparison of the proposed model, the experimental results of the shell-and-tube HX of Backhaus and Swift's thermoacoustic Stirling heat engine (TASHE) [2] is considered.

Table 1. Parameters of the shell-and-tube heat exchanger and working fluid.

Parameter	Symbol	Value	Units
Mean pressure	p_m	3.1	MPa
Mean gas temperature	T_m	319	K
Gas sound speed	a	1060.8	m/s
Gas polytropic coefficient	γ	1.667	-
Gas Prandtl number	σ	0.428	-
Gas thermal conductivity	k	0.159	W/(m·K)
Gas specific heat	c_p	5193	J/(kg·K)
Gas kinematic viscosity	μ	2.08×10^{-5}	kg/(s·m)
HX heat load	\dot{Q}	1614	W
HX length	L_{TAHX}	20	mm
HX thermal conductivity	k_s	14.858	W/(m·K)
HX specific heat	c_s	464.89	J/(kg·K)
HX material density	ρ_s	7909.1	kg/m ³
Operating frequency	f	84	Hz
Gas thermal penetration depth	δ_κ	0.157	mm

In the following sections, the analysis of acoustic energy in shell-and-tube HXs is presented. The TAHXs are considered with a fixed value of heat load. Further, the impact of the geometry configuration (d_i/δ_κ), the TAHX metal temperature (T_s), and the drive ratio (DR) on the acoustic energy dissipation is examined. The optimum value of $(d_i/\delta_\kappa)_{opt}$ as a function of the drive ratio at various T_s is determined. Changes on the acoustic energy dissipation due to the geometry is investigated for different values of T_s . The effect of T_s on the heat exchanger geometry as well as the acoustic energy dissipation is assessed. Moreover, the impact of the drive ratio as an important design parameter is discussed.

The validation of the model is performed by comparing the numerical predictions of the present model with the experimental results of TASHE's shell-and-tube HX [2]. The results are shown in Table 2. As illustrated, regarding the design conditions presented in Table 1, the proposed model can design a shell-and-tube HX and predict the acoustic power dissipated in the HX with good accuracy compared to the shell-and-tube HX of TASHE [2].

Table 2. Comparison of the present model with experimental results of TAHX of TASHE [2] at DR = 0.1 and $T_s = 287$ K.

Parameter	Present Model	TAHX of TASHE [2]	Error (%)
Number of tubes (N_t)	305	299	2%
Tubes diameter (d_t)	2.4 mm	2.5 mm	4%
Acoustic energy dissipation	11.7	12 W	2.5%

3.1. Variation of Acoustic Energy Dissipation (\dot{E}_{diss}) due to Geometry Configuration

The impact of the geometry on acoustic energy dissipation, both viscous and thermal losses, is examined. It should be pointed out that at any T_s of interest, heat exchangers with different configurations (different tube diameters and tube numbers) are designed with maintaining the surface area as constant. Moreover, each configuration can transfer the specified heat load, at the designed T_s with different value of dissipation of acoustic energy.

Figure 1 shows $\dot{E}_{diss,v}$ for the designed shell-and-tube heat exchanger as a function of number of tubes at various T_s , ranging from 270 K to 305 K, for normalized tube diameters (d_i/δ_κ). It can be seen by inspection that, for a fixed T_s , viscous dissipation decreases with increasing d_i/δ_κ and requiring less number of tubes.

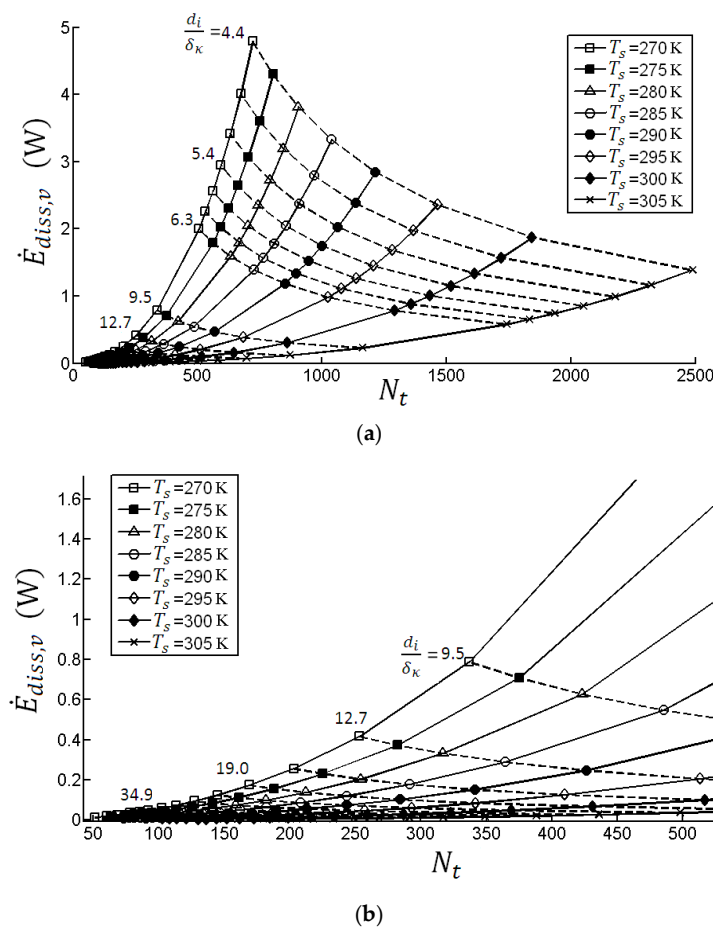


Figure 1. (a) $\dot{E}_{diss,v}$ of the HXs with different N_t and d_i at DR = 0.1; (b) $\dot{E}_{diss,v}$ of the HXs with different N_t and d_i (Zoom for $N_t < 500$).

One may state that at any T_s , the growth of viscous dissipation for heat exchangers with more narrow tubes is associated with the increase of the cross-sectional area of the gas channels in the heat exchanger (A_g) while the heat transfer area (A_s) is kept constant for the specified heat load. Indeed, when the tube diameter decreases in the heat exchanger, the number of the tubes has to be increased to keep the surface area unchanged. However, this triggers a decrease of the A_g which further leads to an increase of the viscous resistance. This is in agreement with Equation (21).

A simulation on $\dot{E}_{diss,\kappa}$ analogous to that of $\dot{E}_{diss,v}$ in Figure 1 is performed. The results are demonstrated in Figure 2. It is evident that $\dot{E}_{diss,\kappa}$ has a different behavior than $\dot{E}_{diss,v}$. At constant T_s , an increase of normalized tube diameter (d_i/δ_κ) has an increasing impact on the thermal dissipation of acoustic power.

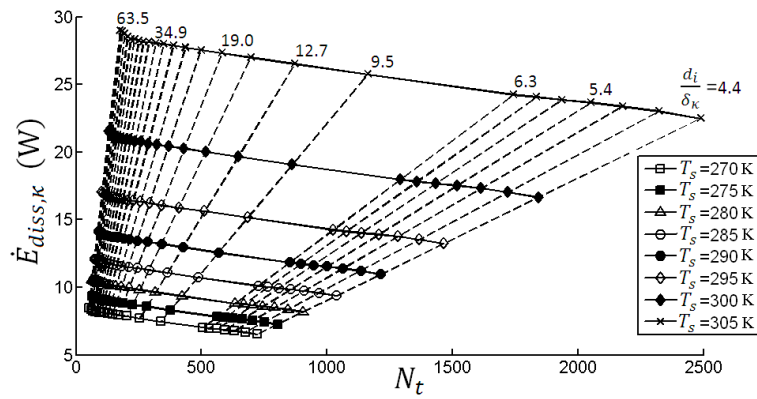
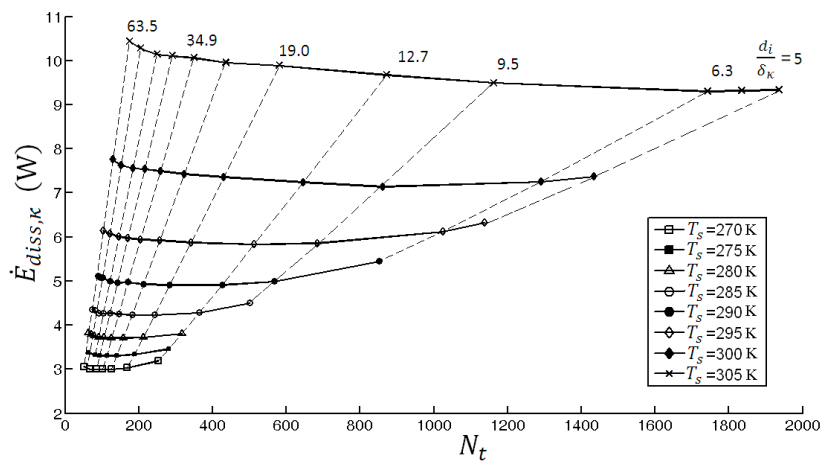
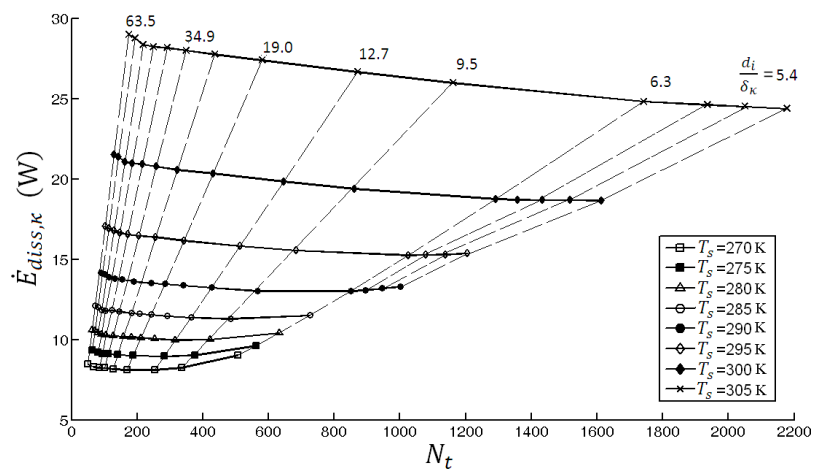


Figure 2. $\dot{E}_{diss,\kappa}$ of the HXs with different N_t and d_i at DR = 0.1.

Considering the different behaviors of $\dot{E}_{diss,\nu}$ and $\dot{E}_{diss,\kappa}$, while viscous dissipation decreases with increasing d_i/δ_κ , thermal relaxation dissipation decreases. A further investigation is made on the impact of the geometric parameters of HXs on the total acoustic energy dissipation. Figure 3 illustrates the total acoustic energy dissipation \dot{E}_{diss} —that is, the combined $\dot{E}_{diss,\nu}$ and $\dot{E}_{diss,\kappa}$ —as a function of number of tubes at various T_s for normalized tube diameter (d_i/δ_κ).



(a)



(b)

Figure 3. \dot{E}_{diss} of the HXs with different N_t and d_i (a) DR = 0.06; (b) DR = 0.1.

A close inspection of the results presented in Figure 3b indicates the existence of a configuration for which the total dissipation, \dot{E}_{diss} , becomes a minimum, $(\dot{E}_{diss})_{min}$. The corresponding normalized tube diameters (d_i/δ_κ) is referred to $(d_i/\delta_\kappa)_{opt}$. In fact, the strong dependence of acoustic energy dissipation on both the number and diameter of the tubes suggests that minimization in acoustic energy dissipation can constitute an effective design criteria to choose the optimal configuration of TAHXs for the given conditions. The optimal TAHXs configuration in correspondence with different operating conditions is presented in Tables 3 and 4. In fact, Tables 3 and 4 are illustrating the shell-and-tube HXs with minimum acoustic energy dissipation $(\dot{E}_{diss})_{min}$ at different T_s values for drive ratios DR = 0.06 and DR = 0.1, respectively.

Table 3. Parameters of optimal shell-and-tube heat exchangers at various T_s at DR = 0.06.

T_s (K)	A_s (m ²)	Re_d (-)	$(\dot{E}_{diss})_{min}$ (W)	$(N_t, d_i)_{opt}$ (-,mm)	$(d_i/\delta_\kappa)_{opt}$ (-)	$(r_h/\delta_\kappa)_{opt}$ (-)
270	0.0325	5167.3	2.98	(92,5.5)	34.9	8.73
275	0.0361	4645.0	3.30	(125,4.5)	28.5	7.14
280	0.0408	4119.2	3.71	(141,4.5)	28.5	7.14
285	0.0467	3593.7	4.23	(208,3.5)	22.21	5.55
290	0.0543	3074.9	4.91	(341,2.5)	15.86	3.97
295	0.0658	2553.4	5.83	(513,2)	12.7	3.17
300	0.0829	2026.1	7.18	(861,1.5)	9.5	2.38
305	0.1118	1503.0	9.31	(1742,1)	6.3	1.59

Table 4. Parameters of optimal shell-and-tube heat exchangers at various T_s at DR = 0.1.

T_s (K)	A_s (m ²)	Re_d (-)	$(\dot{E}_{diss})_{min}$ (W)	$(N_t, d_i)_{opt}$ (-,mm)	$(d_i/\delta_\kappa)_{opt}$ (-)	$(r_h/\delta_\kappa)_{opt}$ (-)
270	0.0325	5167.3	8.12	(203,2.5)	3.97	15.8
275	0.0361	4645.0	8.95	(225,2.5)	3.97	15.8
280	0.0408	4119.2	9.99	(317,2)	3.17	12.7
285	0.0467	3593.7	11.30	(485,1.5)	2.38	9.5
290	0.0543	3074.9	13.03	(567,1.5)	2.38	9.5
295	0.0658	2553.4	15.25	(1025,1)	1.59	6.3
300	0.0829	2026.1	18.37	(1986,0.065)	1.03	4.1
305	0.1118	1503.0	23.40	(2680,0.065)	1.03	4.1

Furthermore, it should be mentioned that the weight of viscous and thermal relaxation losses on the total acoustic energy dissipation is different; thermal relaxation plays the dominant role especially at higher T_s values. A close inspection of Figure 3b reveals that at high T_s values the thermal dissipation of acoustic power is much more than the viscous dissipation; thus, an optimum configuration for which \dot{E}_{diss} becomes a minimum is not available.

Moreover, considering that \dot{E}_{diss} is related to the total time averaged acoustic power dissipation of the heat exchanger, one may state that both the HX metal temperature as well as the drive ratio significantly influence the acoustic power dissipation of shell-and-tube HXs in the travelling-wave engines. The dependence of acoustic energy dissipation on HX metal temperature and the drive ratio are discussed in the following sections.

3.2. The Influence of T_s on Acoustic Energy Dissipation (\dot{E}_{diss})

The influence of T_s on acoustic energy dissipation is further examined. While the viscous dissipation decreases with T_s , the thermal relaxation dissipation increases as shown in Figures 1 and 2, respectively. As it can be seen in Figure 3a,b, the strong dependence of total acoustic energy dissipation on T_s is caused essentially by the thermal relaxation term. The results show that by increasing the T_s ,

larger surface area is needed for heat transfer and consequently the thermal dissipation of acoustic power increases.

Further, it can be seen that both viscous and thermal relaxation dissipations do not vary linearly proportional to T_s . As the temperature difference between the gas and the metal decreases, the acoustic energy dissipation increases progressively.

The design strategy, developed in the previous section and which is based on acoustic energy dissipation minimization, is applied to the model TAHX under study at different operating conditions. At various drive ratios and T_s , the optimal configuration and its corresponding $(\dot{E}_{diss})_{min}$ is determined, Figure 4. It can be seen that an increase of T_s has a minor effect on $(\dot{E}_{diss})_{min}$ at lower drive ratios; however, it has a major effect at larger drive ratios. To be exact, for a TAHX metal temperature of $T_s = 305$ K, an increase of the drive ratio from 0.04 to 0.1 will increase six-fold the total dissipation.

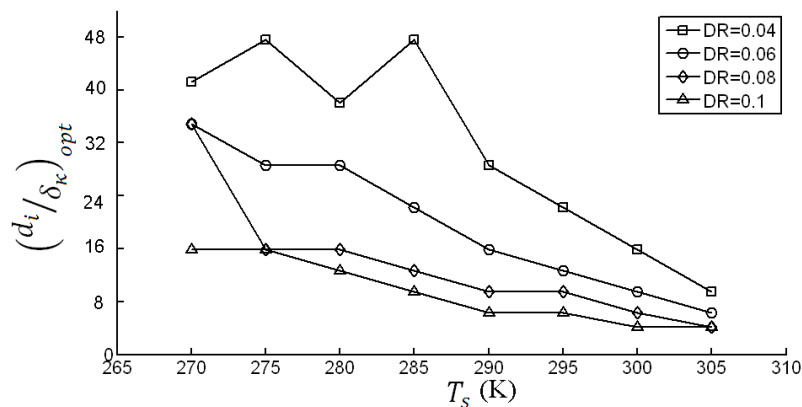


Figure 4. $(\dot{E}_{diss})_{min}$ at any T_s .

The variation of $(d_i / \delta_k)_{opt}$ with T_s at different drive ratios is shown in Figure 5. It is evident that $(d_i / \delta_k)_{opt}$ slightly decreases as T_s increases. This decrease in $(d_i / \delta_k)_{opt}$ has a lower magnitude at larger drive ratios. One may recall that as the TAHX metal temperature increases, the corresponding $(d_i / \delta_k)_{opt}$ decreases—that is, the optimum diameter of the tube decreases. Theoretically, it is possible to obtain an optimum combination between the d_i of the tube and TAHX metal temperature for a minimum acoustic power dissipation.

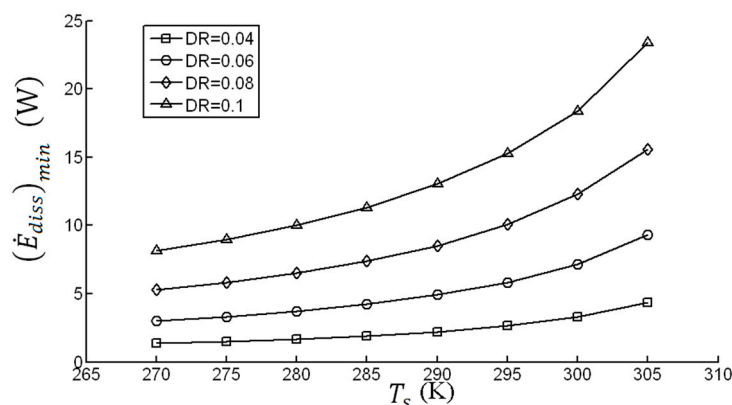


Figure 5. $(d_i / \delta_k)_{opt}$ at various T_s .

The variation of the heat exchanger surface area A_s versus T_s is plotted in Figure 6. It is evident that A_s is proportional to T_s and hence the acoustic power dissipated in the HX and so $(\dot{E}_{diss})_{min}$ is nearly in proportion to T_s . This result is in good agreement with the analysis in Section 2.1—that is, the thermal

relaxation dissipation, which has the biggest impact in total dissipation in the HX, is proportional to A_s .

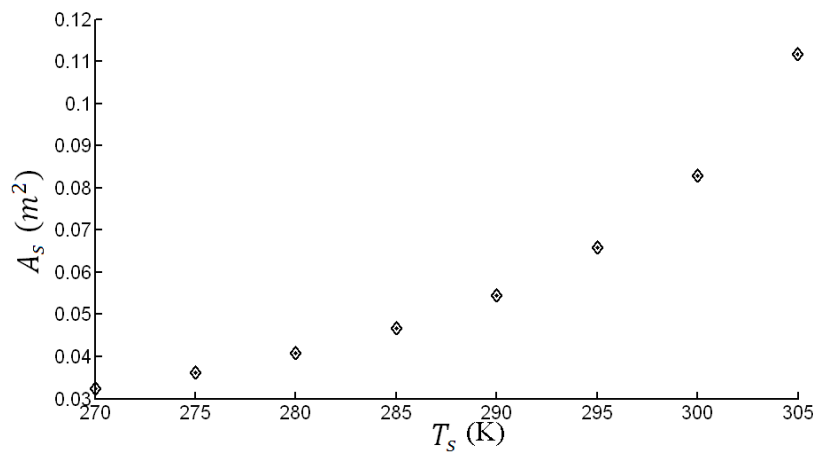


Figure 6. TAHX surface area variation with T_s .

3.3. The Influence of Drive Ratio (DR) on Acoustic Energy Dissipation (\dot{E}_{diss})

Further investigation is made on the impact of the drive ratio on the total acoustic energy dissipation, Figure 3a,b. A comparison between these figures reveals the strong dependency of the total acoustic energy dissipation on the drive ratio. Further, considering the drive ratio as an operating condition, analysis of the influence of drive ratio on the optimal TAHX configuration indicates the increase of the minimum energy dissipation $(\dot{E}_{diss})_{min}$ with the drive ratio. This fact is clearly supported by the rearrangement of the previous results illustrated in Figure 7.

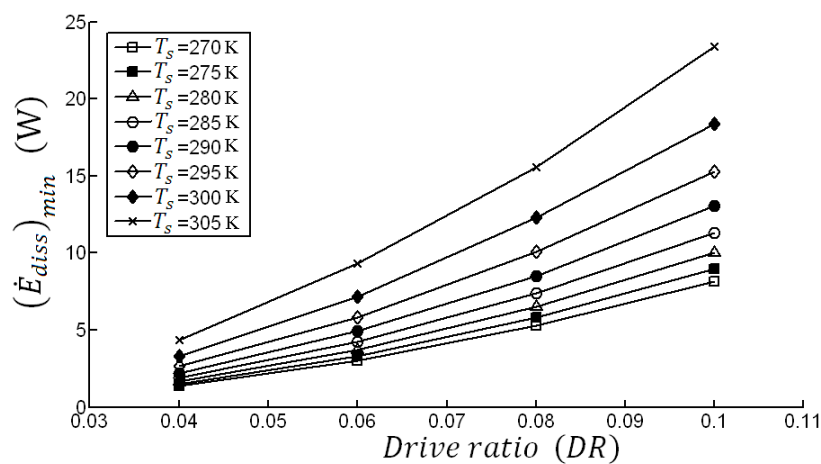


Figure 7. $(\dot{E}_{diss})_{min}$ variation with DR.

Finally, the variation of Reynolds number with TAHX metal temperatures T_s is provided in Figure 8. As mentioned previously, one may specify the values for \dot{Q} , T_m , and T_s to determine A_s , the surface area of the HX. However, different HX configurations (N_t, d_i) might be designed to provide the same A_s . Moreover, since the volume velocity of the gas entering the HX is constant for all the possible configurations, the volume velocity in each tube as well as A_g changes. Nevertheless, Re_d remains constant at each T_s and decreasing the temperature difference between the oscillating gas and the heat exchanger will result in a larger heat transfer area as shown in Figure 6. Further, the increment of heat transfer surface area is provided by increasing the number of tubes, consequently leading to a decrease of Re_d in correspondence with T_s .

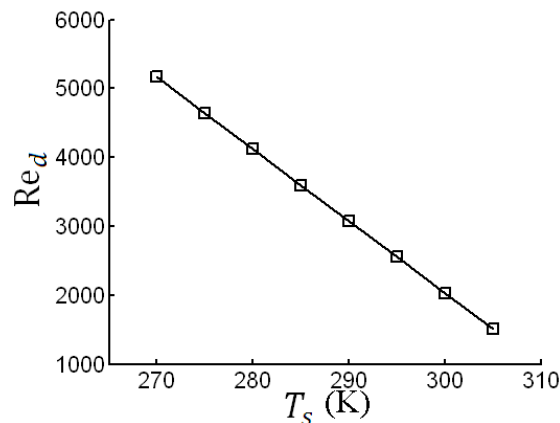


Figure 8. Re_d variation with T_s .

4. Conclusions

Today, thermoacoustic engines, coolers, and heat pumps are gaining more interest for commercialization. While thermoacoustic engines utilize heat to generate acoustic power, the thermoacoustic refrigerators consume the acoustic power to transfer heat from the cold reservoir. A key parameter in making thermoacoustic devices more competitive with classical products is the optimum design of the heat exchangers. Hence, a deeper knowledge of heat exchangers is required so that the gas mean temperature does not change along the flow oscillation and dissipate acoustic energy in the form of viscous and thermal relaxation while transferring the specified heat load.

This research is motivated by developing a simple but constructive methodology for comparison and evaluation of related heat exchangers with respect to acoustic energy dissipation, viscous loss, thermal relaxation loss, tube dimension, and drive ratio. In this paper, the performance of shell-and-tube TAHXs in the travelling-wave mode with ideal gases is investigated through a numerical model based on the classical linear thermoacoustic theory.

The results indicate that, at equal operating conditions, viscous dissipation and thermal relaxation dissipation have opposing behaviors. While $\dot{E}_{diss,v}$ decreases with d_i/δ_k , $\dot{E}_{diss,\kappa}$ increases. Consequently, an optimum value of d_i/δ_k exists, denoted as $(d_i/\delta_k)_{opt}$, at which the total acoustic dissipation becomes a minimum, $(\dot{E}_{diss})_{min}$. The impact of the heat exchanger metal temperature on \dot{E}_{diss} is also investigated. It is determined that, in general, \dot{E}_{diss} increases with T_s . Further, $(d_i/\delta_k)_{opt}$ are obtained to be decreasing with metal temperature T_s . In fact, heat transfer with minimum acoustic energy dissipation at lower temperature defects leads to $d_i \approx \delta_k$. For example, at a drive ratio of 0.06 and metal temperature of 285, the minimum dissipation occurs around $(d_i/\delta_k)_{opt} \approx 16$; whereas at $T_s = 300$ and higher, the minimum dissipation appears at relatively lower d_i/δ_k . The relation between the acoustic energy dissipation and the drive ratio for various T_s is also presented. It is shown that the acoustic energy dissipation increases with the drive ratio. The growth rate, however, was lower for smaller values of T_s .

The proposed model is able to put in evidence the strong dependence of the acoustic energy dissipation on both the diameter and the number of tubes and the existence of minima in correspondence with tube diameter normalized by thermal penetration depth. The different weight of the viscous and thermal losses affecting the HXs behavior is also highlighted with the second one dominating. Also important for design purposes is that acoustic energy dissipation minimization criterion can be effectively employed for the optimization of the configuration of the shell-and-tube TAHXs.

Acknowledgments: The present work has been supported in part by the office of research at Sharif University of Technology.

Author Contributions: Mohammad Gholamrezaei developed the algorithm, provided the results and wrote the draft. Kaveh Ghorbanian was in charge of technical examination and language proficiency. Both authors have read and approved the final manuscript.

Conflicts of Interest: The authors declare no conflict of interest.

Nomenclature

English letters:

a	sound speed	$(\text{m}\cdot\text{s}^{-1})$
A_s	surface area	(m^2)
A_g	cross-sectional area of gas channels	(m^2)
d_o	tube outside diameters	(m)
d_i	tube inside diameters	(m)
DR	drive ratio ($= p_1/p_m$)	-
\dot{E}	acoustic power dissipated	(W)
\dot{E}_{diss}	acoustic power dissipated	(W)
$\dot{E}_{diss,v}$	viscous dissipation of acoustic power	(W)
$\dot{E}_{diss,k}$	thermal dissipation of acoustic power	(W)
\dot{E}_2	time averaged acoustic power	(W)
f	spatially averaged diffusion function	-
f_k	spatially averaged thermal diffusion function	-
f_v	spatially averaged viscous diffusion function	-
g	complex gain/attenuation constant for the volume flow rate	-
h_o	shell-side heat transfer coefficient	$(\text{W}\cdot\text{m}^{-2}\cdot\text{K}^{-1})$
h_i	tube-side heat transfer coefficient	$(\text{W}\cdot\text{m}^{-2}\cdot\text{K}^{-1})$
k	gas thermal conductivity	$(\text{W}\cdot\text{m}^{-1}\cdot\text{K}^{-1})$
L_t	length of the tubes	(m)
L_{TAHX}	optimum length of thermoacoustic heat exchanger	(m)
N_t	number of tube	-
p	Acoustic pressure	(Pa)
p_m	mean pressure	(Pa)
\dot{Q}	heat transfer rate	(W)
r_h	hydraulic diameter	(m)
r_v	viscous resistance per unit length	$(\text{Pa}\cdot\text{m}^{-4}\cdot\text{s})$
r_k	thermal resistance per unit length	$(\text{Pa}\cdot\text{m}^{-4}\cdot\text{s})$
r	acoustic resistance per unit length	$(\text{Pa}\cdot\text{m}^{-4}\cdot\text{s})$
Re_d	tube side acoustic Reynolds number	-
T_{lm}	log-mean temperature	(K)
T	gas temperature	(K)
$T_{w,o}$	water outlet temperature	(K)
$T_{w,i}$	water inlet temperature	(K)
T_0	ambient temperature	(K)
T_m	mean temperature	(K)
U	oscillating volume flow rate	$(\text{m}^3\cdot\text{s})$
U_0	overall heat transfer coefficient	$(\text{W}\cdot\text{m}^{-2}\cdot\text{K}^{-1})$
U_i	overall heat transfer coefficient	$(\text{W}\cdot\text{m}^{-2}\cdot\text{K}^{-1})$
u_1	oscillating velocity	$(\text{m}\cdot\text{s}^{-1})$

Greek symbols:

δ_k	thermal penetration depth	(m)
γ	ratio of isobaric to isochoric specific heats	-
ε	thermal conductivity	(W·m ⁻¹ ·K ⁻¹)
ε_s	correction factor for finite solid heat capacity	-
μ	dynamic viscosity	(kg·m ⁻¹ ·s ⁻¹)
ρ	density of the working gas	(kg·m ⁻³)
σ	Prandtl number	-
ω	angular frequency	(s ⁻¹)
$(\dot{E}_{diss})_{min}$	minimum value of \dot{E}_{diss}	(W)
$(d_i/\delta_k)_{opt}$	optimum value of d_i/δ_k	-

Subscripts:

<i>diss</i>	dissipation
<i>m</i>	mean
<i>min</i>	minimum
<i>opt</i>	optimum
κ	thermal
<i>v</i>	viscous
0	“environment” or “ambient”
1	first order
2	second order

References

- Swift, G.W. Thermoacoustic engines. *J. Acoust. Soc. Am.* **1988**, *84*, 1145–1180. [[CrossRef](#)]
- Backhaus, S.; Swift, G.W. A thermoacoustic Stirling heat engine: Detailed study. *J. Acoust. Soc. Am.* **2000**, *107*, 3148–3166. [[CrossRef](#)] [[PubMed](#)]
- Swift, G.W. *Thermoacoustics: A Unifying Perspective for Some Engines and Refrigerators*; Acoustical Society of America: Melville, NY, USA, 2002.
- Wu, F.; Wu, C.; Guo, F.; Li, Q.; Chen, L. Optimization of a Thermoacoustic Engine with a Complex Heat Transfer Exponent. *Entropy* **2003**, *5*, 444–451. [[CrossRef](#)]
- Zhibin, Y.; Jaworski, A.J. Impact of acoustic impedance and flow resistance on the power output capacity of the regenerators in travelling-wave thermoacoustic engines. *Energy Conv. Manag.* **2010**, *51*, 350–359.
- Tasnim, S.H.; Mahmud, S.; Fraser, R.A. Second law analysis of porous thermoacoustic stack systems. *Appl. Therm. Eng.* **2011**, *31*, 2301–2311. [[CrossRef](#)]
- Chaitou, H.; Nika, P. Exergetic optimization of a thermoacoustic engine using the particle swarm optimization method. *Energy Conv. Manag.* **2012**, *55*, 71–80. [[CrossRef](#)]
- Ishikawa, H.; Hobson, P.A. Optimization of heat exchanger design in a thermoacoustic engine using a second law analysis. *Int. Commun. Heat Mass Transf.* **1996**, *23*, 325–334. [[CrossRef](#)]
- Piccolo, A. Optimization of thermoacoustic refrigerators using second law analysis. *Appl. Energy* **2013**, *103*, 358–367. [[CrossRef](#)]
- Piccolo, A. Numerical Study of Entropy Generation Within Thermoacoustic Heat Exchangers with Plane Fins. *Entropy* **2015**, *17*, 8228–8239. [[CrossRef](#)]
- Swift, G.W.; Backhaus, S. A resonant, self-pumped, circulating thermoacoustic heat exchanger. *J. Acoust. Soc. Am.* **2004**, *116*, 2923–2938. [[CrossRef](#)]
- Incropera, F.P.; DeWitt, D.P.; Bergman, T.L.; Lavine, A.S. *Introduction to Heat Transfer*; John Wiley & Sons: Hoboken, NJ, USA, 2006.

13. Ward, W.C.; Swift, G.W. Design environment for low-amplitude thermoacoustic engines. *J. Acoust. Soc. Am.* **1994**, *95*, 3671–3672. [[CrossRef](#)]
14. Garret, S.L.; Perkins, D.K.; Gopinath, A. Thermoacoustic refrigerator heat exchangers: Design, analysis and fabrication. In Proceedings of the Tenth International Heat Transfer Conference, Brighton, UK, 14–18 August 1994; pp. 375–380.
15. Swift, G.W. Analysis and performance of a large thermoacoustic engine. *J. Acoust. Soc. Am.* **1992**, *92*, 1551–1563. [[CrossRef](#)]
16. Mozurkewich, G. Heat transfer from transverse tubes adjacent to a thermoacoustic stack. *J. Acoust. Soc. Am.* **2001**, *110*, 841–847. [[CrossRef](#)]
17. Paek, I.; Braun, J.E.; Mongeau, L. Characterizing heat transfer coefficients for heat exchangers in standing wave thermoacoustic coolers. *J. Acoust. Soc. Am.* **2005**, *118*, 2271–2280. [[CrossRef](#)]
18. Nsofor, E.C.; Celik, S.; Wang, X. Experimental study on the heat transfer at the heat exchanger of the thermoacoustic refrigerating system. *Appl. Therm. Eng.* **2007**, *27*, 2435–2442. [[CrossRef](#)]
19. Kamsanam, W.; Mao, X.; Jaworski, A.J. Thermal performance of finned-tube thermoacoustic heat exchangers in oscillatory flow conditions. *Int. J. Therm. Sci.* **2016**, *101*, 169–180. [[CrossRef](#)]



© 2016 by the authors; licensee MDPI, Basel, Switzerland. This article is an open access article distributed under the terms and conditions of the Creative Commons Attribution (CC-BY) license (<http://creativecommons.org/licenses/by/4.0/>).